ScholarWorks@UA collection

Seismic moment tensor catalog for local and regional earthquakes recorded in Nenana basin, central Alaska

Kyle Smith

April 12, 2020

Attribution: This file is part of a collection archived at ScholarworksUA (`https://scholarworks.alaska.edu/`) (*Smith*, 2020). It supports a manuscript in preparation for submission *Smith and Tape* (2020).

The seismic data of focus are from the FLATS seismic experiment: Fault Locations from Tectonics And Seismicity, which was supported by the National Science Foundation, Grant EAR-1352668. The seismic network code is XV (*Tape and West*, 2014), and scientific results are presented in *Tape et al.* (2018).

Description of files

A catalog of 33 seismic moment tensors was estimated using body waves and surface waves. The best solution (M_0) was obtained through a random-search in the moment tensor space using the 'cut-and-paste' (CAP) approach, which allows for different frequencies and time shifts on different portions of seismograms (*Zhao and Helmberger*, 1994; *Zhu and Helmberger*, 1996; *Zhu and Ben-Zion*, 2013). The moment tensor approach was adapted and applied in *Silwal and Tape* (2016) for double couple moment tensors and in *Alvizuri and Tape* (2016) for full moment tensors. *Silwal et al.* (2018) updated the misfit function to take into account the polarity error. *Alvizuri et al.* (2018) applied the updated misfit function for estimation of full moment tensors and uncertainties.

A summary of files in the collection is listed in the following table:

figure	description	file name
Figure A1–A33	Waveform fits for 33 events around Nenana Basin	nb_waveforms.pdf
Figure B1–B33	Moment tensor beachballs with input polarity for 33 events around Nenana basin	nb_depth_beach.pdf
Figure C1–C33	time shift and cross-correlation maps for Rayleigh waves and Love waves	nb_depth_beach.pdf
–	text file catalog of 33 moment tensors	nb_mech_kyle.txt
	text file catalog of 48 moment tensors	nb_mech.txt
–	zipped set of text files of input parameters for moment tensor inversions	nb_weights.zip
–	this file: summary of collection	nb_scholarworks.pdf

Within each set of figures (A, B, C), the events are in chronological order by origin time.

Figure A: Waveform fits [nb_waveforms.pdf]

Waveform fits for 33 moment tensor inversions in south-central Alaska. Black are observed waveforms; red are synthetic waveforms computed using a frequency-wavenumber method (*Zhu and Rivera*, 2002) that assumes a (1D) layered model. The waveforms are fit separately within five time windows: P wave vertical component (PV), P wave radial component (PR), Rayleigh wave vertical component (SurfV), Rayleigh wave horizontal component (SurfR), and Love wave transverse component (SurfT). At far left in each row is the station name, source-station distance in km, and station azimuth in degrees. Below each pair of waveforms are four numbers: the cross-correlation time shift between data and synthetics, the cross-correlation value, the percent of the misfit function represented by the waveform pair, and the amplitude ratio between waveforms, $\ln(A_{\text{obs}}/A_{\text{syn}})$, where A is the max value of the waveform within the time window.

The beachball represents the best solution M_0 (i.e., the global minimum of the misfit function). The beachball is plotted as a lower-hemisphere projection (standard seismological convention) of the moment tensor. The surrounding black dots denote the azimuthal location of the stations used, and the red crosses denote the lower hemisphere piercing points of the ray paths to the stations.

Here is a header for an example event in Figure A (see Figure 1 below): The four header lines are as follows:

1. `Event 20190309233958332 Model tactmod Depth 26`
   The event ID is derived from the origin time of 2019-03-09 23:39:58.332.
   The layered model used is `tactmod`, and the event depth is 26 km.

2. `FM 61 66 6 Mw 3.60` γ `0` δ `0 rms 2.497e-01 VR 93.8 pol_wt 0.10`
   The orientation of the moment tensor solution M_0 is strike 61°, dip 66°, rake 6°. (The fault plane of the earthquake could correspond to this triple of angles or to the triple of angles associated with the auxiliary plane.) The estimated magnitude is M_{w} 3.60. The source type of M_0 is expressed in terms of lune longitude $\gamma = 0°$ and lune latitude $\delta = 0°$. Since we are searching only in double couple space, γ and δ are zero for all solutions (see *Alvizuri et al.*, 2018). The waveform difference between data and synthetics is $RMS = 2.497e-01$, and the variance reduction is $VR = 93.8\%$. These are based on a waveform difference measure that rewards using longer time windows and broader bandpass limits. This choice means that the VR cannot be directly compared with VR values reported in other studies. The factor `pol_wt = 0.10` determines the balance between polarity misfit and waveform misfit (i.e., 0.90 for this example). A value of 999.0 means that polarities are not used.

3. `Filter periods (seconds): Body:1.00-4.00. Surf:10.00-25.00 duration: 0.30/0.15 s`
   The body waves were filtered 1–4 s, the surface waves were filtered 10–25 s. In cases where no surface wave are used, the bandpass range is not applicable.
   The source time function is a trapezoidal function whose duration is 0.30 s and whose rise time is half the duration. The duration is not an estimated source parameter but is set according to the target frequency of body waveforms (here 1 Hz). In general, we set the duration to be significantly less than the minimum period used to bandpass-filter the body waves.

4. `# norm L1 # Pwin 8 Swin 80 # N 10 Np 20 Ns 0`
   An L1 norm was used for the misfit function (e.g., *Silwal and Tape*, 2016). The (reference)

P-window is 8 s long and the surface wave window is 80 s long. From a total of 10 stations (N), 20 P wave windows (Np) and 0 surface wave windows (Ns) were used. In this example, surface wave bandpass and window length are not used. For all other events, surface waves were used.

The numbers below each station are:

1. source–station epicentral distance, km
2. station azimuth, in degrees
3. time shift between picked P onset and synthetic P onset.
4. sign of the observed first-motion polarity, which is either 1 (up or compression) or -1 (down or dilatation). The number in parentheses is the predicted amplitude, which ranges between $\pm\sqrt{2}$; numbers close to zero indicate that the station is near a nodal surface of the radiation pattern for the assumed mechanism.

The four numbers below each pair of waveforms are:

1. the cross-correlation time shift $\Delta T = T_{\rm obs} - T_{\rm syn}$ required for matching the synthetics $s(t)$ with the data $u(t)$. A positive time-shift means that the synthetics arrive earlier than the data and that the assumed velocity model is faster than the actual earth structure.
2. the maximum cross-correlation percentage between $u(t)$ and $s(t - \Delta T)$
3. the percentage of the total misfit
4. the amplitude ratio $\ln(A_{\rm obs}/A_{\rm syn})$ in each time window

Figure B-top: Depth search plots [`nb_depth_beach_cap.pdf`]

Figure B-top shows the best-fitting depth grid search for 33 events. An example for one event is shown below as Figure 1 below.

The depth increment for the grid search is 1 km. The red arrow marks the Alaska Earthquake Center catalog depth, and the white arrow marks the depth obtained from the moment tensor inversion. The long tick marks on the x-axis mark the layer boundaries in the 1D model used in the moment tensor inversions. A moment tensor is not permitted to have the same depth as a layer boundary; this is why some beachballs are missing from the depth plots. The 1D model we use is either *tactmod* (*Beaudoin et al.*, 1992; *Ratchkovski and Hansen*, 2002) for events in central Alaska or `scak` (*Matumoto and Page*, 1969; *Lahr*, 1975) for events in southern Alaska. The plot shows the variance reduction (gray curve) with scale on the right. On the left is the variance reduction relative to the minimum variance reduction. The depth uncertainty is calculated based on the depth at which the variance reduction is 0.10 worse than at the best solution. Note that the earthquake magnitude is free to change for each depth, and it generally increases with increasing depth for the best-fitting solution, as we might expect.

Figure B-bottom: Beachballs with ray piercing points [`nb_depth_beach.pdf`]

Here is a header for an example event in Figure B:

The two header lines are as follows:

1. `Event 20190309233958332 Model 20190309233958332_tactmod_026`
   Same as the header line 1 for waveform fits plot.

2. `FM 61 66 6 Mw 3.60` γ `0` δ `0 rms 2.497e-01 VR 93.8 pol_wt 0.10`
   Same as the header line 2 for waveform fits plot.

   The dot ($\cdot$) at the station name outside mark the azimuthal location. The lower hemisphere piercing points are marked with cross (x). The upper hemisphere piercing points are marked with circle (o). For these stations, lower hemisphere piercing point is also marked in (x).

   A triangle is marked instead of (x) for stations with observed polarity specified in the weight file. An observed up polarity is marked with upward pointing triangle; a down polarity is marked with downward pointing triangle. A triangle is colored green or blue if the predicted polarity for the best-fitting moment tensor matches the observed polarity. A triangle is colored red if the predicted polarity for the best-fitting moment tensor does not match the observed polarity.

Figure C: Time shift maps per event

For each event shown in Figure A, we can collect the time shifts for Rayleigh waves and Love waves and plot them as "spider" plots (e.g., *Alvizuri*, 2017; *Alvizuri et al.*, 2018). These plots are useful in assessing the possibility of cycle skipping between observed and synthetic waveforms. Since the time shifts are expected to be caused by differences between real Earth structure and the assumed 1D Earth structure, we expect the time shift patterns to be smoothly varying as the station azimuth changes.

Systematic patterns can be identified. For some time shift maps, the time shifts are solidly positive or negative, indicating that the 1D velocity structure is either too fast or too slow compared to the real Earth structure. We also can identify outlier time shifts and cross-correlations that tend to occur for stations nodal for Rayleigh waves or Love waves. (For a strike-slip fault, a station is nodal for Rayleigh waves if it is in the direction of the fault plane or the auxiliary plane. It is nodal for Love waves if it is in the direction of the P or T axis.)

Text file tables for moment tensor catalogs [`nb_mech.txt` and `nb_mech_kyle.txt`]

Seismic moment tensor catalogs for subset of 33 events and full set of 48 events. Details can be found within the header lines, which also refer to *Kanamori* (1977); *Silver and Jordan* (1982); *Tape and Tape* (2012).

Input text files used in the moment tensor inversion [`nbmt_weights.zip`]

We provide a text file for each of the 33 events in this study. These files show which stations and which time windows were used (or not) in each moment tensor inversion. It also shows the first-motion polarity observations that were used.

References

Alvizuri, C. (2017), Moment tensor catalog results for nuclear explosions, volcanic events, and earthquakes, ScholarWorks@UA at `http://hdl.handle.net/11122/8007` (last accessed 2018-05-09): descriptor file, text files of catalogs, and composite figures of waveform fits, uncertainty results, and time shifts.

Alvizuri, C., and C. Tape (2016), Full moment tensors for small events ($M_{\mathrm{w}} < 3$) at Uturuncu volcano, Bolivia, *Geophys. J. Int.*, *206*, 1761–1783, doi:10.1093/gji/ggw247.

Alvizuri, C., V. Silwal, L. Krischer, and C. Tape (2018), Estimation of full moment tensors, including uncertainties, for nuclear explosions, volcanic events, and earthquakes, *J. Geophys. Res. Solid Earth*, *123*, 5099–5119, doi:10.1029/2017JB015325.

Beaudoin, B. C., G. S. Fuis, W. D. Mooney, W. J. Nokleberg, and N. I. Christensen (1992), Thin, low-velocity crust beneath the southern Yukon-Tanana terrane, east central Alaska: Results from Trans-Alaska Crustal Transect refraction/wide-angle reflection data, *J. Geophys. Res.*, *97*(B2), 1921–1942.

Kanamori, H. (1977), The energy release in great earthquakes, *J. Geophys. Res.*, *82*, 2981–2987.

Lahr, J. C. (1975), Detailed Seismic Investigation of Pacific–North American Plate Interaction in Southern Alaska, Ph.D. thesis, Columbia University, New York City.

Matumoto, T., and R. A. Page (1969), Microaftershocks following the Alaska earthquake of March 28, 1964: Determination of hypocenters and crustal velocities in the Kenai Peninsula-Prince William Sound area, in *The Prince William Sound, Alaska, Earthquake of 1964 and Aftershocks*, vol. II, Parts B and C, edited by L. E. Leipold and F. J. Wood, pp. 157–173, U.S. Department of Commerce, Environmental Science Services Administration, Washington, D.C., U.S. Coast and Geodetic Survey Publication 10-3.

Ratchkovski, N. A., and R. A. Hansen (2002), New constraints on tectonics of interior Alaska: Earthquake locations, source mechanisms, and stress regime, *Bull. Seismol. Soc. Am.*, *92*(3), 998–1014, doi:10.1785/0120010182.

Silver, P. G., and T. H. Jordan (1982), Optimal estimation of scalar seismic moment, *Geophys. J. R. Astron. Soc.*, *70*, 755–787.

Silwal, V., and C. Tape (2016), Seismic moment tensors and estimated uncertainties in southern Alaska, *J. Geophys. Res. Solid Earth*, *121*, 2772–2797, doi:10.1002/2015JB012588.

Silwal, V., C. Tape, and A. Lomax (2018), Crustal earthquakes in the Cook Inlet and Susitna region of southern Alaska, *Tectonophysics*, *745*, 245–263, doi:10.1016/j.tecto.2018.08.013.

Smith, K. (2020), Seismic moment tensor catalog for local and regional earthquakes recorded in Nenana basin, central Alaska, ScholarWorks@UA at `http://hdl.handle.net/XXXX/XXXX` (last accessed April 2020): descriptor file, text file of catalog, figures with waveform fits, and input weight files.

Smith, K., and C. Tape (2020), Seismic response of Nenana sedimentary basin, central Alaska, *Bull. Seismol. Soc. Am.* (in prep.).

Tape, C., and M. E. West (2014), Fault Locations and Alaska Tectonics from Seismicity, International Federation of Digital Seismograph Networks. Other/Seismic Network. `doi:10.7914/SN/XV_2014`.

Tape, C., S. Holtkamp, V. Silwal, J. Hawthorne, Y. Kaneko, J. P. Ampuero, C. Ji, N. Ruppert, K. Smith, and M. E. West (2018), Earthquake nucleation and fault slip complexity in the lower crust of central Alaska, *Nature Geoscience*, *11*, 536–541, doi:10.1038/s41561-018-0144-2.

Tape, W., and C. Tape (2012), A geometric setting for moment tensors, *Geophys. J. Int.*, *190*, 476–498, doi:10.1111/j.1365-246X.2012.05491.x.

Zhao, L.-S., and D. V. Helmberger (1994), Source estimation from broadband regional seismograms, *Bull. Seismol. Soc. Am.*, *84*(1), 91–104.

Zhu, L., and Y. Ben-Zion (2013), Parameterization of general seismic potency and moment tensors for source inversion of seismic waveform data, *Geophys. J. Int.*, *194*, 839–843, doi: 10.1093/gji/ggt137.

Zhu, L., and D. Helmberger (1996), Advancement in source estimation techniques using broadband regional seismograms, *Bull. Seismol. Soc. Am.*, *86*(5), 1634–1641.

Zhu, L., and L. A. Rivera (2002), A note on the dynamic and static displacements from a point source in multilayered media, *Geophys. J. Int.*, *148*, 619–627, doi:10.1046/j.1365-246X.2002.01610.x.

Table 1: Source parameters estimated for 33 events recorded in Minto Flats. The index in the second column corresponds to the set of 48 events in Table 1 of *Smith and Tape* (2020). The third column for depth and magnitude is the difference AEC – CAP, where AEC is the Alaska Earthquake Center catalog value and CAP is our value estimated from the moment tensor inversion of filtered seismic waveforms.

		origin time	longitude	latitude	depth, km			magnitude					
					CAP	AEC		M_w	M_l		strike	dip	rake
1	23	2015-12-02 10:05:25.798	-147.2622	61.6966	39	36.59	-2.4	3.75	4.50	0.75	69	79	29
2	26	2016-01-18 04:05:56.098	-150.6400	62.1032	18	10.09	-7.9	4.55	4.50	-0.05	159	67	35
3	35	2016-05-15 05:51:00.219	-150.9465	63.0765	135	131.54	-3.5	5.25	5.30	0.05	55	61	74
4	17	2016-05-18 03:25:48.320	-151.0651	65.2466	12	15.16	3.2	4.10	4.20	0.10	349	47	-18
5	25	2016-05-21 11:34:09.789	-152.4627	62.3598	135	143.49	8.5	4.50	4.52	0.02	351	86	84
6	20	2016-07-11 20:05:57.702	-149.2282	63.8056	120	123.05	3.0	4.20	4.10	-0.10	99	44	36
7	16	2016-11-06 09:29:10.579	-150.0626	64.1639	21	23.19	2.2	4.00	4.00	0.00	22	67	-10
8	22	2016-12-08 10:18:13.868	-150.0376	64.1937	21	24.52	3.5	4.35	4.30	-0.05	21	86	-17
9	34	2017-02-13 07:17:12.642	-142.7477	62.5120	12	8.86	-3.1	5.20	5.10	-0.10	48	90	-5
10	27	2017-04-29 11:15:48.898	-151.1656	63.1225	16	11.90	-4.1	4.80	4.90	0.10	315	34	11
11	1	2017-05-27 16:33:05.640	-149.2261	64.6896	17	18.02	1.0	3.20	3.30	0.10	227	66	-23
12	14	2017-06-13 07:39:36.181	-148.2574	63.8685	106	101.25	-4.8	3.95	3.90	-0.05	85	58	2
13	3	2017-06-28 12:58:51.897	-148.9082	64.7566	19	17.30	-1.7	3.30	3.30	0.00	238	54	8
14	6	2017-11-08 06:49:11.318	-148.6552	64.8620	16	16.80	0.8	3.55	3.70	0.15	18	71	-45
15	33	2017-11-27 22:18:30.467	-147.4303	60.5552	30	16.62	-13.4	5.20	5.30	0.10	216	83	-79
16	12	2017-12-30 11:43:16.278	-149.0240	63.8011	6	7.12	1.1	3.90	4.00	0.10	41	84	27
17	18	2018-01-19 23:55:05.310	-148.9897	63.9765	137	129.27	-7.7	4.15	4.60	0.45	131	67	4
18	2	2018-08-25 18:15:51.481	-149.2033	64.6164	17	19.91	2.9	3.20	3.19	-0.01	40	24	-26
19	21	2018-08-28 15:18:43.464	-150.5718	65.1780	16	16.92	0.9	4.30	4.70	0.40	6	89	7
20	9	2018-09-16 19:11:54.565	-151.3493	65.1562	12	15.50	3.5	3.70	3.88	0.18	215	69	7
21	15	2018-10-03 03:29:37.544	-148.9191	64.8979	19	19.69	0.7	4.00	3.94	-0.06	250	38	30
22	28	2018-10-14 23:53:14.769	-156.3956	67.7739	16	10.53	-5.5	4.85	5.00	0.15	319	74	-61
23	30	2018-10-27 16:57:28.350	-151.5744	65.2283	15	14.84	-0.2	4.90	5.10	0.20	171	81	-36
24	13	2018-11-13 15:26:41.907	-150.9466	64.7938	16	17.65	1.7	3.95	4.10	0.15	217	81	-18
25	31	2019-01-13 16:45:55.437	-150.0647	61.2993	48	44.83	-3.2	4.90	5.30	0.40	200	76	-79
26	7	2019-01-17 12:13:55.493	-149.0340	64.2410	17	17.21	0.2	3.55	3.73	0.18	33	77	5
27	32	2019-03-06 21:33:13.991	-157.2186	66.3108	2	9.09	7.1	5.05	5.30	0.25	353	88	-2
28	8	2019-03-09 23:39:58.332	-147.7368	64.5498	26	26.50	0.5	3.60	3.61	0.01	61	66	6
29	29	2019-03-26 21:27:18.519	-157.2445	66.2996	6	9.79	3.8	4.90	5.10	0.20	160	73	-39
30	19	2019-04-11 10:42:45.609	-149.1761	64.7370	17	19.86	2.9	4.15	4.53	0.38	198	72	-11
31	4	2019-06-24 09:04:23.195	-149.8657	64.2797	19	20.61	1.6	3.35	3.36	0.01	39	48	-21
32	24	2019-09-06 23:32:28.461	-152.3552	64.6032	8	11.81	3.8	4.25	4.57	0.32	192	86	-16
33	11	2019-09-25 13:45:13.442	-149.2576	63.7657	16	12.16	-3.8	3.85	4.07	0.22	193	84	6

Table 2: Input parameters for moment tensor inversions. All events used a $\Delta M_w = 0.05$ magnitude search except 2018-08-25 which used 0.01. "bp" = bandpass for filtering, "dur" = duration, and "P times" indicates whether P arrival times from the AEC catalog were used or not (this can help reduce cycle-skipping by restricting the allowable time shifts).

		origin time	mag	dur	bp body		bp surf		depth search			P	1D
			M_w	s	s	s	s	s	km	km	km	times	model
1	23	2015-12-02 10:05:25.798	3.75	1.00	1.5	4.0	16.0	40.0	30	45	1	N	scak
2	26	2016-01-18 04:05:56.098	4.55	1.00	2.0	4.0	16.0	40.0	1	30	1	N	scak
3	35	2016-05-15 05:51:00.219	5.25	0.50	0.5	2.0	16.7	40.0	120	150	1	N	tactmod
4	17	2016-05-18 03:25:48.320	4.10	0.20	1.0	3.0	20.0	40.0	5	25	1	Y	tactmod
5	25	2016-05-21 11:34:09.789	4.50	1.00	1.5	4.0	16.0	40.0	130	155	1	N	scak
6	20	2016-07-11 20:05:57.702	4.20	1.00	1.0	3.0	10.0	20.0	110	135	1	N	tactmod
7	16	2016-11-06 09:29:10.579	4.00	1.00	1.5	4.0	16.0	40.0	5	35	1	N	tactmod
8	22	2016-12-08 10:18:13.868	4.35	1.00	1.5	4.0	16.0	40.0	5	35	1	N	tactmod
9	34	2017-02-13 07:17:12.642	5.20	0.20	1.5	4.0	16.0	40.0	1	25	1	Y	scak
10	27	2017-04-29 11:15:48.898	4.80	0.50	1.0	3.0	16.0	40.0	1	32	1	N	tactmod
11	1	2017-05-27 16:33:05.640	3.20	0.50	1.0	2.5	10.0	18.0	5	30	1	N	tactmod
12	14	2017-06-13 07:39:36.181	3.95	0.50	1.0	3.0	10.0	25.0	90	110	1	Y	tactmod
13	3	2017-06-28 12:58:51.897	3.30	0.20	1.0	3.0	16.0	30.0	5	30	1	Y	tactmod
14	6	2017-11-08 06:49:11.318	3.55	0.50	1.0	3.0	10.0	25.0	5	30	1	N	tactmod
15	33	2017-11-27 22:18:30.467	5.20	0.20	1.5	4.0	16.0	40.0	10	45	1	Y	scak
16	12	2017-12-30 11:43:16.278	3.90	0.50	1.0	2.5	10.0	20.0	1	20	1	N	tactmod
17	18	2018-01-19 23:55:05.310	4.15	1.00	1.5	4.0	16.0	40.0	120	145	1	N	tactmod
18	2	2018-08-25 18:15:51.481	3.20	0.20	1.0	3.0	16.0	40.0	5	30	1	Y	tactmod
19	21	2018-08-28 15:18:43.464	4.30	1.00	1.5	4.0	16.0	40.0	10	24	1	Y	tactmod
20	9	2018-09-16 19:11:54.565	3.70	0.50	1.0	2.5	10.0	25.0	5	25	1	Y	tactmod
21	15	2018-10-03 03:29:37.544	4.00	1.00	1.5	4.0	10.0	50.0	10	30	1	N	tactmod
22	28	2018-10-14 23:53:14.769	4.85	1.00	2.0	4.0	16.0	40.0	1	35	1	Y	tactmod
23	30	2018-10-27 16:57:28.350	4.90	1.00	1.5	4.0	10.0	50.0	8	24	1	N	tactmod
24	13	2018-11-13 15:26:41.907	3.95	1.00	1.5	4.0	16.0	30.0	5	30	1	Y	tactmod
25	31	2019-01-13 16:45:55.437	4.90	1.00	1.5	4.0	16.0	40.0	30	60	1	N	scak
26	7	2019-01-17 12:13:55.493	3.55	0.50	1.0	3.0	10.0	18.0	10	30	1	N	tactmod
27	32	2019-03-06 21:33:13.991	5.05	0.50	1.5	4.0	16.0	40.0	1	25	1	Y	tactmod
28	8	2019-03-09 23:39:58.332	3.60	0.30	1.0	4.0	10.0	25.0	20	40	1	Y	tactmod
29	29	2019-03-26 21:27:18.519	4.90	0.50	1.5	3.0	16.0	40.0	1	25	1	Y	tactmod
30	19	2019-04-11 10:42:45.609	4.15	0.50	1.0	3.0	16.0	40.0	5	25	1	N	tactmod
31	4	2019-06-24 09:04:23.195	3.35	0.50	1.0	3.0	10.0	20.0	10	30	1	N	tactmod
32	24	2019-09-06 23:32:28.461	4.25	0.50	1.0	2.5	16.7	50.0	2	20	1	N	tactmod
33	11	2019-09-25 13:45:13.442	3.85	0.50	1.0	2.5	10.0	20.0	1	25	1	N	tactmod

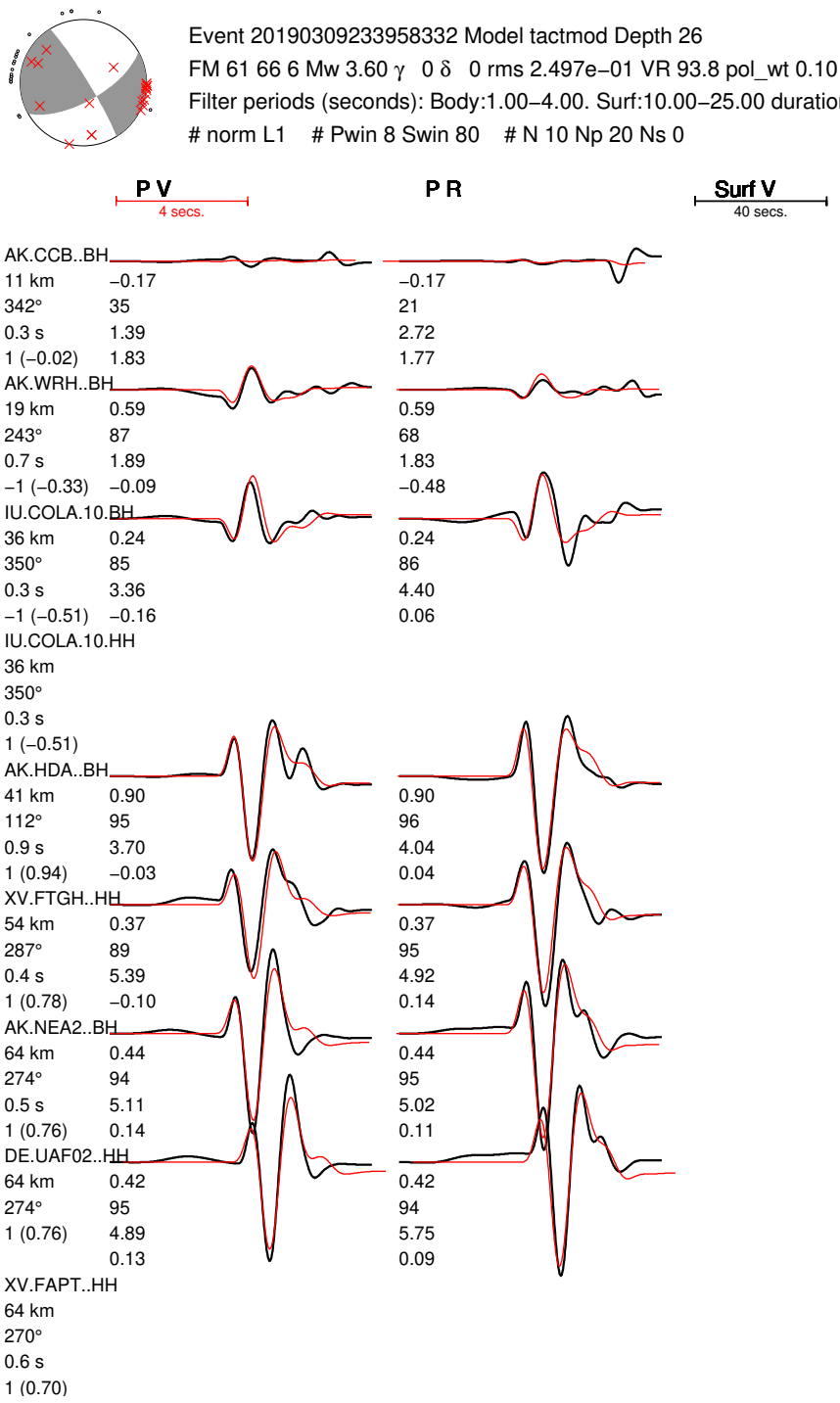

Figure 1: Waveform fits between data (black) and synthetic (red) seismograms. This event (20190309233958332) is an outlier in the sense that it is one of the few events where 1) surface waves could not be used due to poor signal-to-noise levels, and 2) first-motion polarity measurements were used to help constrain the solution. This appears as Figure A28 within the concatenated pdf.

a

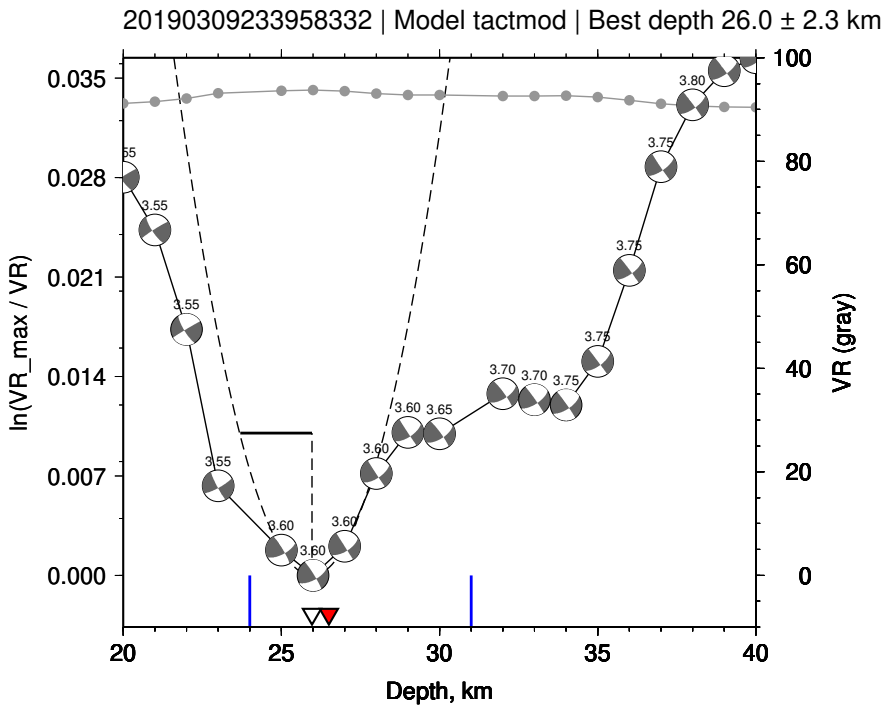

b

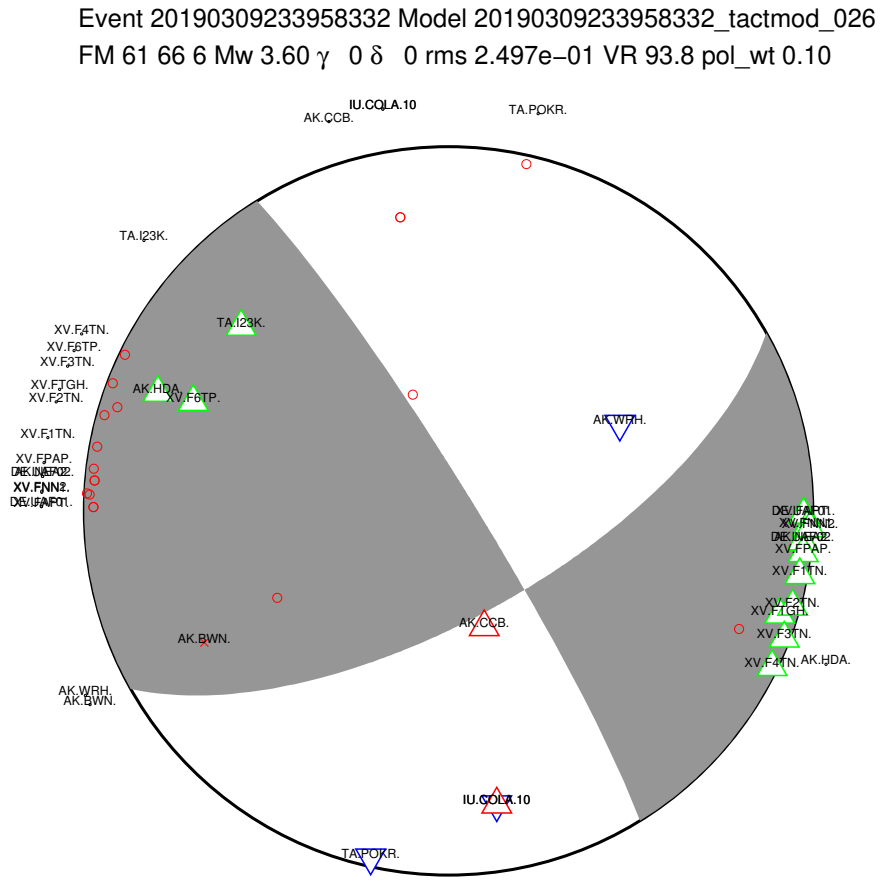

Figure 2: Depth grid search (a) and best-fitting moment tensor (b) associated with the waveform fits in Figure 1. This appears as Figure B28 within the concatenated pdf.